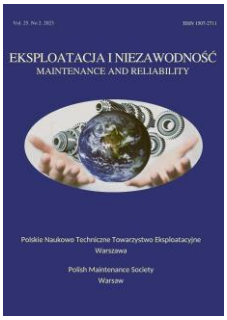

Eksploatacja i Niezawodnosc – Maintenance and Reliability
Volume 28 (2026), Issue 3
journal homepage: http://www.ein.org.pl

Article citation info:
Li Z, Tian X, Du H, Xia L, Han J, Algebraic parameterization-based spiral machining toolpath generation for C^1-continuous compound surfaces, Eksploatacja i Niezawodnosc – Maintenance and Reliability 2026: 28(3) http://doi.org/10.17531/ein/218673

Algebraic parameterization-based spiral machining toolpath generation for C^1-continuous compound surfaces

Indexed by: Web of Science Group

Zining Li[a,b], Xiaoqing Tian[a,b,*], Hao Du[a,b], Lian Xia[a,b], Jiang Han[a,b]

[a] School of Mechanical Engineering, Hefei University of Technology, Hefei, 230009, China
[b] Anhui Engineering Laboratory of Intelligent CNC Technology and Equipment, Hefei, 230009, China

Highlights

- Generate control curves for spiral tool paths via Coons reparameterization.
- Form spiral tool paths on Coons surfaces by head-to-tail connection.
- Rebuild 2D compound UV domain via Coons mapping to ensure G^1 continuity.

Abstract

In the CAM machining of complex surfaces such as open blisk blades, unsmooth tool paths often occur at the common boundaries of compound surfaces. Conventional parameter alignment cannot guarantee C^1 continuity in the Euclidean parameter domain. To generate boundary-consistent spiral tool paths on compound or trimmed surfaces, a method based on Coons reparameterization is proposed for computing the control lines required to generate spiral tool paths. On the unfolded Coons compound surfaces, spiral tool paths are generated directly by connecting the start and end points, avoiding the need to compute 3D points one by one. However, this may still fail to ensure C^1 continuity at surface boundaries. Therefore, a 2D compound parameter domain is reconstructed via Coons mapping, which maintains the geometric features of the part and ensures C^1-continuous tool paths at common boundaries. Simulation and machining of an open blisk blade verify the method's effectiveness, showing improved contour accuracy and an 18% reduction in surface roughness after optimization.

Keywords
compound surfaces, trimmed surfaces, spiral machining toolpaths, Coons patch, C^1 continuity

1. Introduction

In the current five-axis CNC machining, the machining parts are often shaped with complex surfaces, and in the machining parts, such as the open blisk, the open blisk blade surface is generally divided into ruled and free-form surfaces [1]. The ruled surface processing method is relatively simple, while the free-form surface CNC machining programming is relatively complex. Complex surfaces like free-form are generally smoothly combined from multiple parametric surfaces at their common boundary. In the process of machining parts with complex surfaces, such as the open blisk, the tool path is usually required to comply with the boundary consistency; that is, when machining the boundary curve, the machining tool path should transition smoothly without lifting the tool and other operations [2]. This toolpath offers a more aesthetically pleasing and smoother appearance for complex parts with compound surfaces.

Many efforts have been made to study the generation of tool paths for the five-axis machining of complex compound surfaces. Various methods have been developed, including iso-planar [3], iso-parametric [4], iso-scallop [5,6], and mesh-based [7,8]. Among them, the iso-planar and iso-parametric methods are relatively more straightforward, mature, and thus widely

(*) Corresponding author.
E-mail addresses: Z. Li (ORCID: 0009-0001-0528-9072) 2021170196@mail.hfut.edu.cn, X. Tian (ORCID: 0000-0002-4589-922X) tianxiaoqing@hfut.edu.cn, H. Du, duhao.hfut@gmail.com, L. Xia, xialian@hfut.edu.cn, J. Han, jianghan@hfut.edu.cn

used. However, the above two methods cannot generate consistent tool paths with consistent boundaries for trimmed or compound free-form surfaces when the machined part surfaces require a certain degree of smoothness and better aerodynamic performance. Specifically, in the iso-parametric method, when generating toolpaths from trimmed surfaces, such as those on the open blisk blade, intersections of iso-parametric lines with the blade top cause toolpath discontinuities. This necessitates the addition of non-cutting movements during machining, resulting in inconsistent toolpath boundaries and increased processing time. Mesh-based approaches are commonly employed for toolpath generation in machining. However, for complex surface parts, such as open blisks, this method typically represents them as parametric surfaces and must therefore be discretized into mesh models prior to toolpath generation. This discretization process inevitably leads to surface accuracy loss [9], while mesh-mesh intersection and offset operations incur significant computational cost. Surface reparameterization is currently widely adopted to achieve consistent and smooth transitions in the machining toolpaths along the boundaries of compound surfaces. Various methods have been proposed by Yang et al. [10,11] to address this problem. One of the proposed methods is to fit the parameter domain with Coons surfaces, and the tool paths with consistent boundaries can be generated by using a two-step mapping method with the help of iso-parametric lines of Coons surfaces. Chuang et al. [12]. used two-bit Laplace parameterization and original Laplace parameter redistribution for cavity tool paths to generate boundary-consistent tool paths. However, these methods are limited to single free-form surfaces. Many researchers have also explored methods for generating toolpaths for multiple compound surfaces. Keigo et al. [13] generated tool paths with constant pitch and spiral paths in the parameter domain by creating machining points that preserve the distance information between corresponding points in Euclidean space, extending to surfaces composed of multiple patches. The proposed method utilizes parameter boundaries to represent the connection relationship between the boundaries of each surface on the parameter domain. However, this method cannot generate a streamlined tool path; Xu et al. [14] proposed an offset method for polyhedral surface curves, thereby facilitating data exchange and geometric computation of polyhedral surfaces. However, there is insufficient information about the method's performance and specific implementation. Han et al. [15] used a reparameterization method to generate spiral tool paths on free-form surfaces, effectively ensuring surface accuracy and roughness for complex parts. However, this approach involves calculating the position of each point to build the spiral tool path, resulting in relatively low computational efficiency. Regarding the issues above, boundary-consistent toolpath generation methods based on reparameterization, especially the 2D Coons surface reparameterization, are considered. In this method, a parametric surface is inputted, and the 2D parametric domain of the surface is first fitted with a 2D Coons surface, followed by a two-step mapping to generate boundary-consistent control lines through the iso-parametric lines of the Coons surface. Finally, the spiral cutter contact line is calculated using the control line, and the cutter contact points are discretely generated within the chordal height constraint. On the unfolded Coons compound surface, spiral tool paths are generated directly by connecting endpoints, eliminating the need to individually locate three-dimensional points along the spiral path in Euclidean space. This method generates consistent and homogeneous toolpaths, but after projecting the CC (Cut Contact) curves mapped by the Coons surface onto the original compound surface, the accuracy and smoothness of the original toolpaths differ on the compound surface, and the continuity is usually not guaranteed, which does not ensure good machining accuracy.

Maharavo et al. [16] used arc-length parameterization for 2D Coons mapping and the function images of binary function combinations of trimmed surfaces to ensure continuity by matching point by point at the common boundary, but could not guarantee the accurate computation of the arc-length curves after reparameterization; Mario et al. [17] conducted a detailed analysis of the C^1-smooth, geometrically continuous, and isogeometric function space for bilinear parameterized two-sided surface domains, and proved the correlation between function construction and the geometric continuity of surfaces. However, this method can only be used to construct surfaces with two surface domains. To address these issues and limitations, this study adopts the idea of building a G^1 parameterization suitable for analysis, as proposed in [18]. It ensures that the newly constructed parameter domains have the

exact boundaries, vertices, and first-order derivatives at the vertices as the original parameter domains, according to the method of [19], to make the two as close as possible.

In this study, the parametric mapping is transferred into the Coons parameter domain, and the boundary of the parameter domain after reparameterization is interpolated with B-splines. Finally, B-spline basis functions represent the compound surface. The compound parameter domain is reconstructed to achieve G^1 continuity, ensuring that the compound surface C^1 in Euclidean space is continuous. Through simulation and processing verification, it is proven that the method can provide good continuity of the paths at the common boundary of the compound surface.

2. Surface reparameterization method

A compound surface comprises multiple surface patches smoothly connected at a common boundary. Such surface patches can be either simple surfaces or trimmed surfaces. A schematic diagram of the paths at the common boundary of the compound surface is shown in Fig. 1, where Fig.1(a) shows the tool path with G^1 continuity at the common boundary of the compound surface and Fig.1(b) shows the tool path with G^0 continuity at the common boundary of the compound surface. Denote the entire compound surface of the parameter domain as φ. For each patch, e.g., each edge on the surface of the ith patch φ^i is denoted as $\partial\varphi^i = \{\alpha_{i,1}, \alpha_{i,2}, \cdots, \alpha_{i,j}\}$, where j is the number of boundaries on φ^i. In the compound surface φ^i, the common boundaries of φ^1 and φ^2 are $\alpha_{1,2}(\alpha_{2,4})$. The boundary-consistent tool paths of the compound surfaces are generally streamlined, meeting the requirements of the uppermost and lowermost boundary compounds of φ^i. This representation of the common boundary defines connectivity.

Optimizing continuity at the common boundary of a compound surface presented in Section 4 of this paper first ensures that the compound surface in Euclidean space is C^1-continuous. The endpoints (p, q) and the first endpoints (p', q') on the corresponding isoparametric lines in two neighboring parameter domains coincide. Otherwise, it is impossible to generate smooth tool paths with G^1 continuity on the parameter domain of the compound surface. Fig. 1(a)(b) shows the case of having the same point overlap at the common boundary $\alpha_{1,2}(\alpha_{2,4})$of different parameter domains.

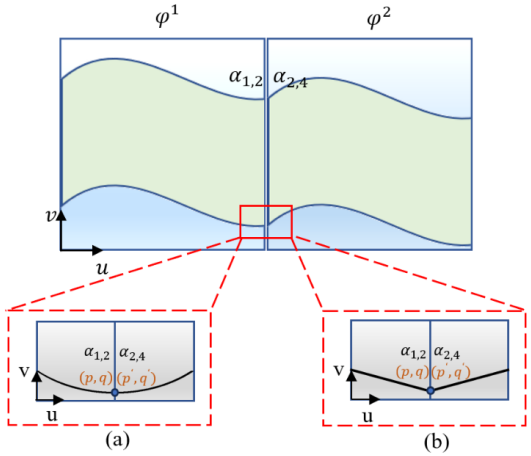

Figure 1. Schematic of the common boundary of the compound surface (a) Tool path with G^1 continuity (b) Tool path with G^0 continuity.

The parameter domains of different trimmed surfaces may differ if the $n+1$th parameter domains adjacent to the nth parameter domain are directly considered as the intersection points with the boundary along the iso-parametric lines in the nth parametric domain. In such cases, the points with the same value at the common boundary of two different parameter domains may not overlap due to the differing ranges of parameter domains values. The iso-parametric line on the surface of the second parameter domain is insignificant. As shown in Fig. 2, $D_0, D_1, D_0', D_1'; C_0, C_1, C_0', C_1'$ are the boundary curves in the corresponding parameter domains of the surface. These are expressed using NURBS (non-uniform rational B-splines), and the parameter ranges of the boundary curves are not necessarily [0,1] in the trimmed surface, when $n = 2$, let the parameter ranges of these eight curves are in order

$$[w_{D_0}, l_{D_0}], [w_{D_1}, l_{D_1}], [w_{C_0}, l_{C_0}], [w_{C_1}, l_{C_1}]; [w'_{D_0}, l'_{D_0}], [w'_{D_1}, l'_{D_1}], [w'_{C_0}, l'_{C_0}], [w'_{C_1}, l'_{C_1}],$$

where w and l denote the parameter values representing the starting and ending points of $D(s)$ and $C(t)$, respectively, within their trimmed surface parameter domains. The four corner points of the corresponding parameter domains of the two surfaces are $P_{00}, P_{01}, P_{10}, P_{11}; P'_{00}, P'_{01}, P'_{10}, P'_{11}$. When taking the value of ω on the first parameter domain boundary curve and the value of ω' on the second parameter domain, if the two neighboring parameter domains take the same range of values ω and ω' coincide, otherwise ω and ω' don't coincide at the common boundary. The C^0-continuous tool path can't be obtained at the boundary of the compound parameter domain.

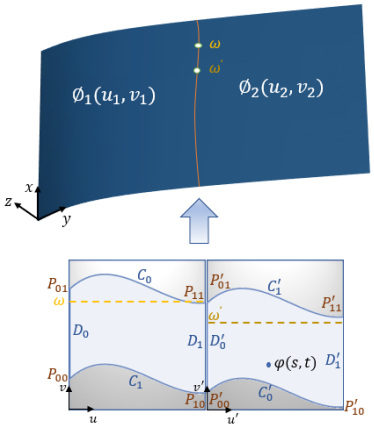

Figure 2. Schematic diagram of boundary curves of different parameter domains and the value ranges.

To obtain tool paths with overlapping endpoints at the common boundary of the compound surface and to ensure that the iso-parametric lines maintain the same proportional positions when taking the same value in different parameter domains, a method based on the Coons interpolation algorithm is proposed to reparameterize the parameter domains of the compound surfaces. The specific flow is shown in Fig. 3.

Using the four boundary curves and four corner points of each surface, the bilinear Coons surface of a single trimmed surface $P(s,t)$ in a two-dimensional compound surface in the UV parameter domain is represented as:

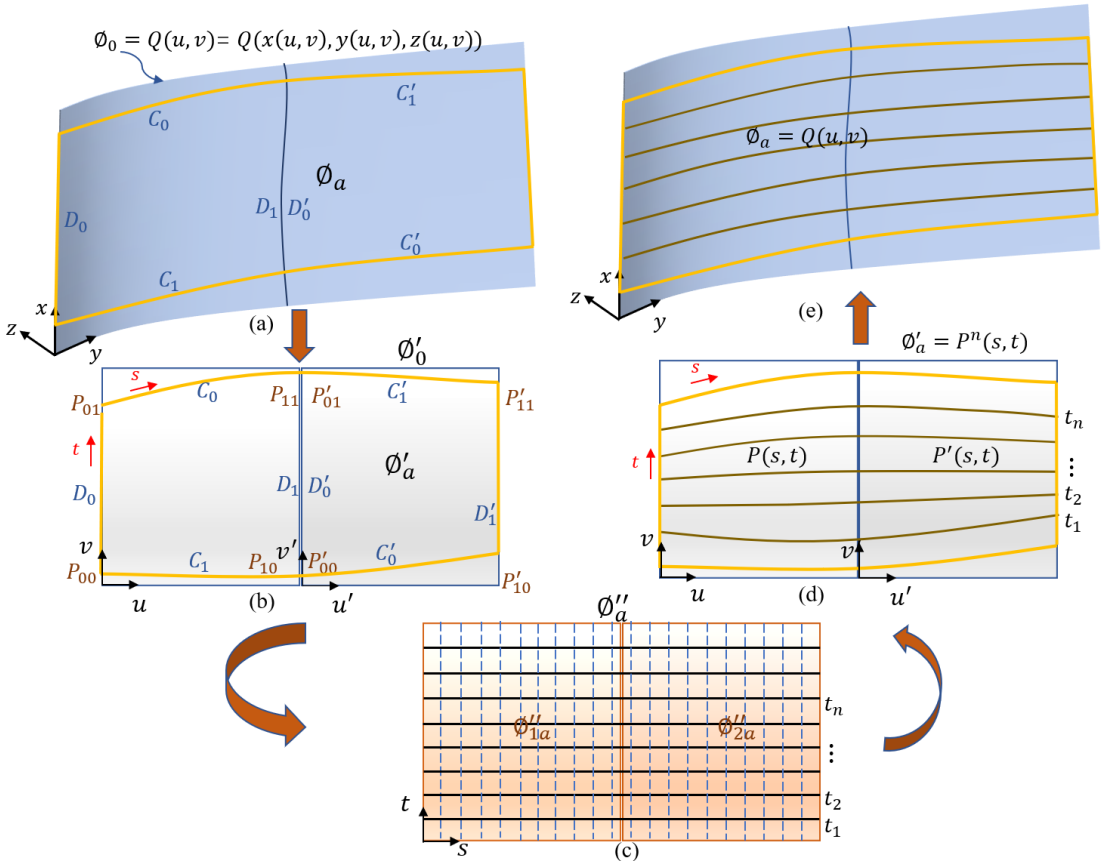

Figure 3. Two-stage mapping for endpoint overlap tool path generation.

$$P(s,t) = P_A(s,t) + P_B(s,t) - P_C(s,t) \quad (1)$$

$$P_{\mathcal{A}}(s,t) = [1-s \quad s]\begin{bmatrix} D_0(w_{D_0} + t(w_{D_0} - l_{D_0})) \\ D_1(w_{D_1} + t(w_{D_1} - l_{D_1})) \end{bmatrix} \quad (1a)$$

$$P_B(s,t) = \begin{bmatrix} C_0(w_{C_0} + s(f_{C_0} - l_{C_0})) \\ C_1(w_{C_1} + s(f_{C_1} - l_{C_1})) \end{bmatrix}^T \begin{bmatrix} 1-t \\ t \end{bmatrix} \quad (1b)$$

$$P_C(s,t) = [1-s \quad s]\begin{bmatrix} P_{00} & P_{01} \\ P_{10} & P_{11} \end{bmatrix}\begin{bmatrix} 1-t \\ t \end{bmatrix} \quad (1c)$$

Similarly, the bilinear Coons surface representation of an adjacent trimmed surface $P'(s,t)$ in a two-dimensional compound surface is expressed as follows:

$$P'(s,t) = P_A'(s,t) + P_B'(s,t) - P_C'(s,t) \quad (2)$$

$$P_{\mathcal{A}}'(s,t) = [1-s \quad s]\begin{bmatrix} D_0'(w_{D_0}' + t(w_{D_0}' - l_{D_0}')) \\ D_1'(w_{D_1}' + t(w_{D_1}' - l_{D_1}')) \end{bmatrix} \quad (2a)$$

$$P_B'(s,t) = \begin{bmatrix} C_0'(w_{C_0}' + s(f_{C_0}' - l_{C_0}')) \\ C_1'(w_{C_1}' + s(f_{C_1}' - l_{C_1}')) \end{bmatrix}^T \begin{bmatrix} 1-t \\ t \end{bmatrix} \quad (2b)$$

$$P_C'(s,t) = [1-s \quad s]\begin{bmatrix} P_{00}' & P_{01}' \\ P_{10}' & P_{11}' \end{bmatrix}\begin{bmatrix} 1-t \\ t \end{bmatrix} \quad (2c)$$

The resulting Coons surface patches $P^n(s,t)$ realizes the reparameterization of the parameter domain of a single trimmed

surface. $P^n(s,t)$ covers the region of the compound surface within the two-dimensional parameter domain, thus mapping the irregular surface parameter domain onto a rectangular parameter domain. Additionally, the parameter ranges for different rectangular domains are all s∈ [0,1], $t \in [0,1]$. Since compound surface patches match at their shared boundaries, in the Coons parameter domain:

$$\phi''_{1a} \cap \phi''_{2a} \in \partial\phi''_a \tag{3}$$

Fig. 3(c) illustrates the Coons compound parameter domain with the identical common boundary $\partial\emptyset''_a$.

3. Iso-parametric discrete toolpath generation

The tool paths generated by the iso-parametric method are based on curves [20]. In the case of a compound surface consisting of trimmed surfaces, each surface is represented using the B-spline method. The trimmed surface $\emptyset(u,v)$ in the Euclidean space is expressed as:

$$\emptyset(u,v) = \frac{\sum_{i=0}^{m}\sum_{j=0}^{n}\omega_{ij}p_{ij}N_{i,k}(u)N_{j,l}(v)}{\sum_{i=0}^{m}\sum_{j=0}^{n}\omega_{ij}N_{i,k}(u)N_{j,l}(v)}, 0 \le u,v \le 1 \tag{4}$$

Where, p_{ij} denotes a three-dimensional control point on the trimming surface, $N_{i,k}(u)$ and $N_{j,l}(v)$ represent the kth and lth B-spline basis functions of the surface, respectively, and ω_{ij} is the weighting factor for the surface. After reparameterization on the compound surface, the first step is to determine the interval between two consecutive tool paths, where the scallop height constrains the interval. The path interval is calculated based on the corresponding longest iso-parametric line segmented by the scallop height.

3.1. Generation of iso-parametric lines in Euclidean space

The process of generating a toolpath for a compound surface should be initiated by specifying the location of the first toolpath. Any curve on the surface can be used as the starting toolpath, but the boundary curve of the first surface is typically selected as the initial toolpath of the compound surface. In the parameter domain of the Coons surface {s∈ [0,1], t ∈ [0,1]}, take the iso-t lines as shown in Fig. 4(a), so that $t_m = o.5$, and s start from 0 with ε as a step（$0 < \varepsilon < 1$）. A series of two-dimensional points $P_i(s_n, t_m)$ are obtained on the Coons surface by cyclic computation. The 2D points are mapped by B-spline curve fitting to obtain the curve C_{m2} in the UV parameter domain. The mapped points are $Q_i(s_n, t_m)$, the NURBS curve expression for C_{m2} is:

$$C_{m2}(u) = \frac{\sum_{i=0}^{n}\omega p_i N_{i,k}(u)}{\sum_{i=0}^{n}\omega_i N_{i,k}(u)}, 0 \le u \le 1 \tag{5}$$

Where, d_i denotes a control point, ω_i represents the weight of the control point, and $N_{i,k}(u)$ indicates the kth B-spline basis function of the surface. The boundary of the parameter domain of the trimmed surface is represented by a thick solid line, as shown in Fig. 4(b).

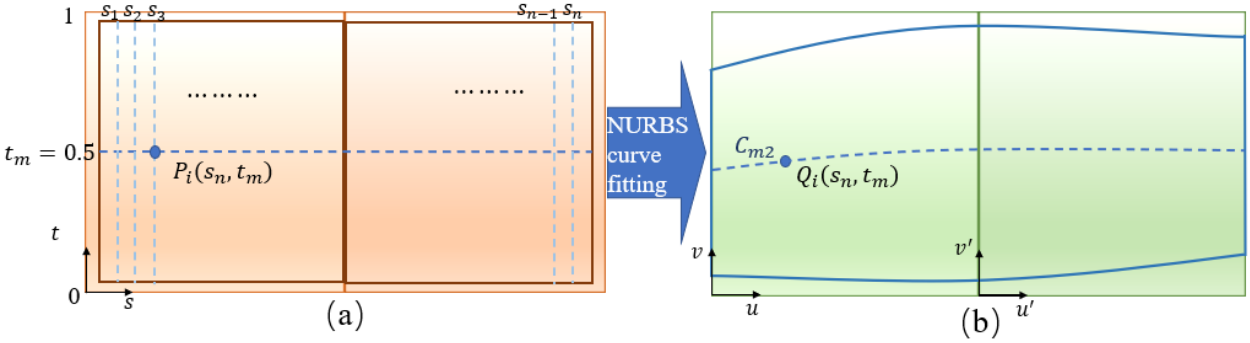

Figure 4. Compound surface parameter domain iso-t line generation process (a) Schematic of compound Coons surface parameter domain iso-s/t line (b) Schematic of iso-t line on the compound surface parameter domain.

The curve C_{m2} in the UV parameter domain is mapped into the Euclidean space to obtain the curve C_m. The first point (x_0, y_0, z_0) and the last point (x_n, y_n, z_n) are found at the boundary of the surface C_m, and the other CC points are solved by recursion. Calculate the arc length s between two neighboring points according to the formula and the chord height e, where the step length f is calculated as:

$$f \le 2\sqrt{2eR + e^2} \tag{4}$$

$$R = \frac{\|[r_u \; r_v][u_t \; v_t]^T\|}{\|[r_{uu} \; r_{uv} \; r_{vv}][u_t{}^2 \; u_t v_t \; v_t{}^2]^T\|} \tag{5}$$

To more accurately determine the actual 3D points on the compound trimmed surface in xyz 3D space, the arc length s between neighboring 3D points is used for recursive derivation instead of the step length f. For the curve C_m in

Euclidean space, a series of 3D points is obtained by discretization using the chord height constraint, and the arc length s is calculated as:

$$s = \begin{cases} f, when\ k_n = 0 \\ 2R\ arg sin(\frac{f}{2R}), when\ k_n \neq 0 \end{cases} \quad (6)$$

Where k_n is the normal curvature of the surface at the point, R is the radius of curvature of the curve at the point, f is the straight line distance between two neighboring points, i.e., the step length, and the chord height is set to a constant e.

Through the above calculation, the three-dimensional points on the curve C_m can be determined sequentially. The points on C_{m2} are solved cyclically based on the mapping relationship between the arc length s between the two points and the parameters of the curve C_{m2} in the UV parameter domain. The final point Q_i is shown in Fig. 4(b). The mapping relationship between each point and the points on the iso-t line of the Coons surface has been constructed. The golden section search algorithm (GSS) [21] is used to improve the efficiency and accuracy of the results, and the algorithm is formulated as follows:

$$f(s_n) = \|P_i(s_n, t_m) - Q_i\|^2 \quad (7)$$

GSS finds the maximum or minimum value of the unimodal function by narrowing the search space [22], and in this study, iteratively calculates the value of s_n when the value of $f(s_n)$ is the minimum value for the corresponding. At this point, the points on the iso-t line in the Coons surface parameter domain are denoted as (s_n, t_m). According to the calculated s_n, get the iso-s line in the parameter domain of Coons surface. According to the mapping, the curve in the UV compound parameter domain is obtained, as shown in Fig. 5. The obtained curves are discretized according to the chord height constraints, and the discrete points (m_i, n_i) are obtained.

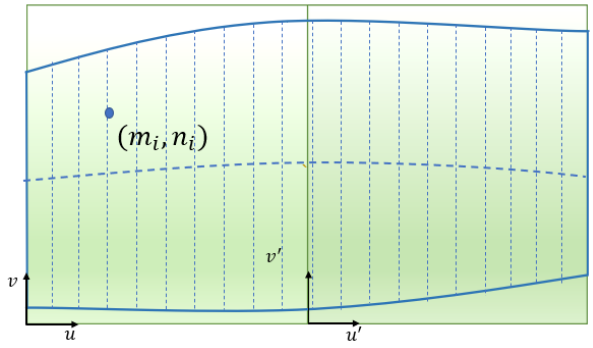

Figure 5. Iso-s line in the parameter domain of the surface under chord height constraints.

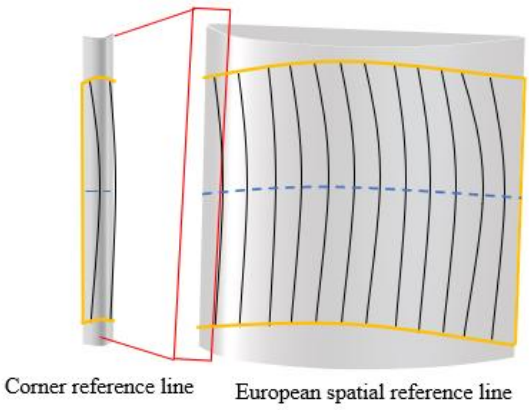

Figure 6. Schematic diagram of 3D surface reference lines and reference lines at corners in Euclidean space.

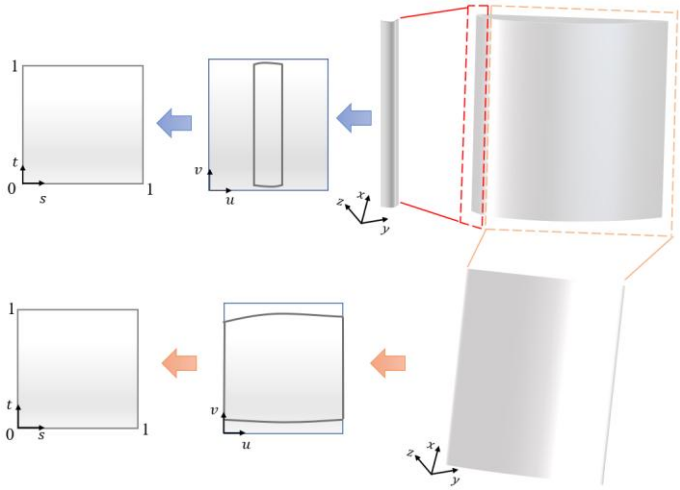

Figure 7. Two-stage mapping of regions with varying curvature.

Calculate the coordinates of the discrete point (m_i, n_i) in Euclidean space to determine the point locations. Fit a B-spline curve to these points, resulting in a series of curves constrained by chord heights, as shown in Fig. 6. The reference lines at corners correspond to the shared boundary curves of two neighboring surfaces within a compound surface. This area often shows the most noticeable parameter inconsistencies and mapping distortions [23]. In this study, the Coons reparameterization method directly maps surfaces in the UV parameter domain to the Coons surface parameter domain, as shown in Fig. 7. Surfaces at high-curvature locations, such as blade corners and edges, and at low-curvature locations, such as the blade face, are ultimately mapped to the Coons parameter domain with a range of [0,1] to generate tool paths. In the Coons reparameterization toolpath generation method, surface curvature is not introduced as an explicit variable in the parameter mapping or toolpath generation process. Instead,

toolpath generation is primarily governed by the parametric mapping relationships and does not directly depend on variations in curvature magnitude. As shown in Fig. 6, since the compound surfaces meet at the common boundary, the reference line at the corners maintain a smooth geometric transition in Euclidean space. Therefore, the reference line on the compound surface demonstrates excellent reliability and robustness.

3.2. Spiral machining tool path generation

The reference line obtained in Section 3.1 is discretized into a set of points with an equal number to generate a spiral machining tool path on a compound surface. First, find the longest reference line and discretize the reference line into n segments with the maximum scallop height h_{max} as the distance between adjacent points. The set of points on the longest reference line in the Euclidean space is obtained as $\{\emptyset_1, \cdots \emptyset_i\}$. Then, the discrete point set is mapped to the parameter domain to get the point set $\{Q_1, \cdots Q_i\}$ on the parameter domain and finally mapped to the Coons surface parameter domain to obtain the iso-s line. The point set is denoted as $\{P_1 \cdots P_i\}$. As shown in Fig. 8.

Draw the iso-t lines based on the spacing between the points $\{P_1 \cdots P_i\}$ on the iso-s line, $t \in \{t_1, \cdots, t_n\}$, respectively. These n iso-t lines are connected head to tail in Euclidean space, i.e., a chain of torus points. To generate a toroidal point chain on a compound Coons surface, identify the first and last points of the neighboring iso-t lines and connect them to obtain a series of inclined straight lines, these lines are then mapped to Euclidean space to get a toroidal point chain. Then the spiral machining tool paths are obtained through B-spline curve fitting, as shown in Fig. 9.

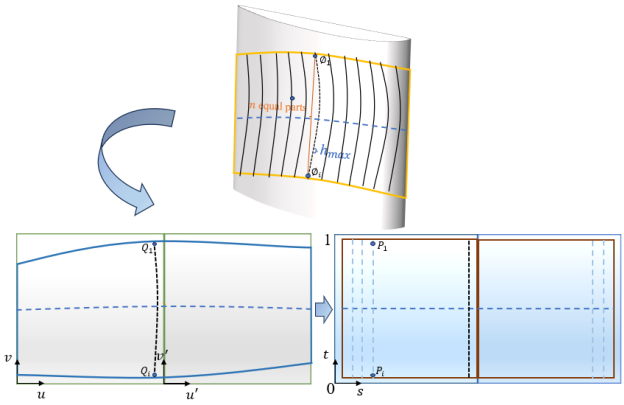

Figure 8. Discrete point generation on Coons' compound parametric surface under maximum scallop height constraints.

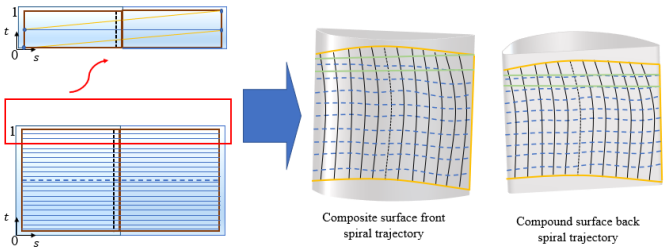

Figure 9. Schematic diagram of Coons compound parameter domain iso-t line generation and spiral machining tool path generation in Euclidean space.

4. Optimization of continuity

The Coons-based method described above creates spiral tool paths on compound surfaces in Euclidean space. However, the generated paths do not necessarily ensure C^1 continuity at the junctions of composite surfaces. Sun et al. [24] proved that to make the cross-border trajectories on a compound surface first-order continuous, the compound surface must be C^1-continuous. The operator space is set to $S_k^{p,\gamma}(\omega)$ according to the method of [19], where p is the order of the spline function (in each direction). k determines the number of uniform interior nodes in each direction, with continuity C^r at all the interior nodes, r is the degree of smoothness at each interior node, and the multiplicity of the interior nodes is defined as $p-r$. where $k \in \mathbb{Z}_0^+, 0 \le r \le p$, and let $n = p + k(p-\gamma)$. If the spline space is denoted as $S_k^{p,r}([0,1]^2)$ and consists of B-splines, it is denoted as $N_{i,j}^{p,r} = N_i^{p,r} N_j^{p,r}$. A Coons surface-based reparameterization of the 2D parameter domain has been performed in Section 3 to ensure that the paths have a consistent parameterized form in the parameter domain. From Section 2, the combined patches in the UV parameter domain are φ, $\varphi \in R^d$, where any two patches overlap only at their boundary. Let the first surface be denoted as τ and the second surface as τ'. The overlapping boundary between surfaces τ and τ' is expressed as:

$$\varphi^{(\tau)} \cap \varphi^{(\tau')} \in \partial\varphi^{(\tau,\tau')} \tag{8}$$

The parameter domain after reparameterization is $F^{(\tau)}([0,1]^2), \tau \in \{1, \cdots, n\}$, and the common boundary is:

$$F^{(\tau)} \cap F^{(\tau')} \in \partial F^{(\tau,\tau')} \tag{9}$$

The common boundary parametrization of Eq. (11) is denoted as $\partial F^{(\tau,\tau')}: [0,1] \to R^2$. Two patches in the parameter domain share the entire common boundary curve $\partial F^{(\tau)}$, i.e., these two patches are neighboring patches. To introduce the non-uniform node vectors of each pair of neighboring patches

$F^{(\tau)}$, $F^{(\tau')}$ into the C^0-continuous spline space, it is sufficient to match the node vectors of any two neighboring patches. Moreover, the parameterization has the same boundary $\partial F^{(\tau)}$ at $s = \rho$,**Błąd! Nie można odnaleźć źródła odwołania.** when:

$$\partial F^{(\tau,\tau')} = \{F^{(\tau)}(\rho,t) = F^{(\tau')}(\rho,t), t \in [0,1]\} \quad (10)$$

When interpolating B-spline curves along each of the four given boundaries u and v directions of a Coons surface, and the boundary curves are defined through the control point P_{ij}, the surface can be approximated in B-spline form at this time [25], so according to the paper [19] the idea has:

$$F(s,t) = \sum_{i=0}^{n}\sum_{j=0}^{n} P_{ij}\, N_{ij}(s,t) \quad (11)$$

A non-uniform knot vector spline space is introduced when the knot vectors on any two adjacent patches match. Fig. 10 shows the schematic of the compound surface F-mapping.

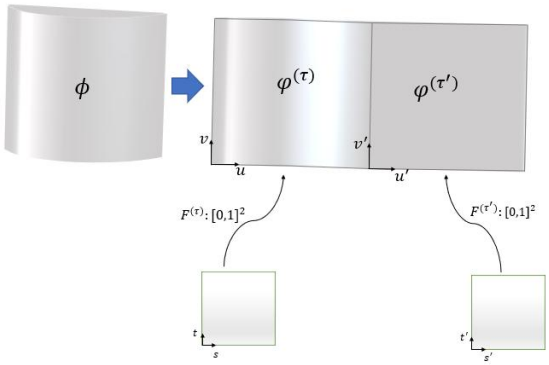

Figure 10. Schematic diagram of compound patches mapping.

4.1. G^1 parameterization suitable for analysis

Sun et al. [24] proposed that the compound surface in three-dimensional space is C^1-continuous, and the path can be made C^1-continuous at the common boundary of the compound surface in three-dimensional space by ensuring G^1-continuous in the two-dimensional parameter domain. To avoid singularities in parameter mapping, there should be:

$$det[\, D_s F(i)(s,t) D_t F(i)(s,t)] \neq 0 \quad (12)$$

This formula guarantees the regularity of the parameterization such that the tangential directions f_τ, $f_{\tau'}$ of two adjacent surfaces $F^{(\tau)}$ and $F^{(\tau')}$ are aligned after reparameterization. As shown in the Fig.11.

In two neighboring parametrized surfaces $F^{(\tau)}$ and$F^{(\tau')}$, at the boundary $\partial F^{(\tau)}$, if there exists $\alpha^{(\tau)}$: $[0,1]$, $\alpha^{(\tau')}$: $[0,1]$, and β: $[0,1]$, and all the values are within the real number R, such that for all $t \in [0,1]$, there are:

$$\alpha^{(\tau)}\alpha^{(\tau')} < 0 \quad (13)$$

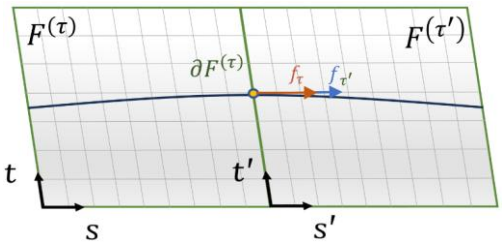

Figure 11. Schematic of tangential directions f_τ and $f_{\tau'}$ for two adjacent surfaces $F^{(\tau)}$ and $F^{(\tau')}$ after reparameterization.

The sign condition in Eq. (15) prevents cusps from appearing on the general surface. In determining the continuity of the path of a compound surface in the parameter domain, gluing data $\alpha^{(\tau)}$, $\alpha^{(\tau')}$, and β play a critical role, and Eq. (16) ensures that the surface transitions smoothly at the common boundary.

$$\alpha^{(\tau')}(t) D_s F^{(\tau)}(\rho,t) - \alpha^{(\tau)}(t) D_s F^{(\tau')}(\rho,t) + \beta(t) D_t F^{(\tau,\tau')}(t) = 0 \quad (14)$$

Where,

$$\beta(t) = \alpha^{(\tau)}\beta^{(\tau')}(t) - \alpha^{(\tau')}\beta^{(\tau)}(t) \quad (15)$$

$\beta^{(\tau)}$ and $\beta^{(\tau')}$ are one-parameter function families, see [18,26]. At this point the parameterized compound parameter domain satisfies the G^1 condition for being suitable for analysis.

4.1. Continuous construction of compound surface G^1 based on reparameterization

In this study, we apply a method to construct a parametric domain G1-continuous from a polyhedron with a compound surface, in which a G1-continuous path can be generated in the parametric domain by taking a point at the same scale at the beginning and the end of the compound surface and connecting them. After reparameterization, the new parameter domain is specified as φ° , and the compound surface is parametrically mapped as F° ,_which is mapped by n regular geometries $F^{\circ(l)} \in S_{k^\circ}^{p^\circ r^\circ}([0,1]^2) \times S_{k^\circ}^{p^\circ r^\circ}([0,1]^2)$, $1 \le r^\circ \le p^\circ$, where $p^\circ \ge 1$, $k^\circ \ge 0$.

According to the method in Section 4, the same parameterization is consistent at $s = \rho$, as shown in Eq (18):

$$F^{\circ(\tau)}(\rho,t) = F^{\circ(\tau')}(\rho,t), t \in [0,1], \rho \in [0,1] \quad (16)$$

Currently, the reparameterized adjacent surface patches are C^0 continuous along their common boundary. We find the parametric mapping F, where $F^{(\tau)} \in S_k^{p,r}([0,1]^2) \times S_k^{p,r}([0,1]^2)$, consisting of compound patches. To achieve G^1 continuity across the common boundary, it must have $S_k^{p,r}([0,1]^2) \supseteq$

$S_{k^\circ}^{p^\circ\, r^\circ}$ ($[0,1]^2$). The space is then refined further to encompass the parametric space of the specified compound patches. Moreover, more restrictive constraints are applied to the continuity order and continuity, specifically $1 \le r \le p-2$. When F is as close as possible to F° ,the two-dimensional parameter domain φ has G^1 continuity.

To make $F \approx F^\circ$, first make the boundaries of the two 2D parameter domains coincide, which is:

$$\partial\varphi = \partial\varphi^\circ \tag{17}$$

And at and at $\tau \in \{1, \cdots, n\}$. The reparameterized $F^{(\tau)}$ and $F^{\circ\,(\tau)}$ vertices at the vertices as well as the first-order derivatives coincide and have:

$$F^{(\tau)}(s_0,t_0) = F^{\circ\,(\tau)}(s_0,t_0),\ D_sF^{(\tau)}(s_0,t_0) = D_sF^{\circ\,(\tau)}(s_0,t_0),$$
$$D_tF^{(\tau)}(s_0,t_0) = D_tF^{\circ\,(\tau)}(s_0,t_0) \tag{18}$$

At this point $s_0, t_0 \in \{0.1\}$. When the reparameterized patches are all regular, the above condition ensures that the 2D parameter domain satisfies G^1 continuity.

For the constructed G^1-continuous compound surface, the gluing data $\alpha^{(\tau)}$, $\alpha^{(\tau')}$, β should satisfy the linear constraints on the control point $P_{ij}^{(\tau)}$ where the control point $P_{ij}^{(\tau)}$ is the point in the parameterization $F^{(\tau)}$, $\tau \in \{1, \ldots, p\}$. It is also necessary that the interface $\partial\varphi^{(\tau,\tau')}(s,t)$ at the boundary of the compound surface satisfies the sign conditions of Eq. (15), ensuring no singularities on the surface. And the gluing data satisfy constraints (12) (16) (17), it is also necessary to have:

$$\alpha^{(\tau)}(s_0) = \alpha^{\circ\,(\tau)}(s_0),\ \alpha^{(\tau')}(s_0) = \alpha^{\circ\,(\tau')}(s_0),\ \beta(s_0) = \beta^\circ(s_0) \tag{19}$$

where $s \in [0,1]$, when for the interface $\partial\varphi^{(\tau,\tau')}(s,t)$ at the boundary. To impose strict G^1 continuity conditions on the common boundary of cthe ompound patch, the method from **Błąd! Nie można odnaleźć źródła odwołania.** is used to generate the necessary linear constraints for the gluing data with respect to control points $P_{ij}^{(\tau)}$. The initial parameterization F° and gluing data $\alpha^{(\tau)}(s_0)$, $\alpha^{(\tau')}(s_0)$, $\beta(s_0)$ ensure tangential consistency at the interfaces between adjacent faces. Boundary constraints guarantee that the reparameterized compound parameter domains F and F° share common boundaries, achieving boundary consistency. At each vertex of the surface patch, position and first-order derivatives are continuous, with vertex constraints preventing singularities at vertices.

In this study, the initial parameterization F° can be generated directly without the need of externally provided parameterization because of a fixed interface $F^{\circ\,(\tau)}(\rho,t) = F^{\circ\,(\tau')}(\rho,t)$ on the parameter domain. At this point, the initial parameterized compound patch parameterization is obtained by minimizing the objective function, which can be calculated from [19] as follows:

$$\lambda_L F_L(d^{\circ\ \tau}_{ij}) + \lambda_U F_U(d^{\circ\ \tau}_{ij}) \to min \tag{20}$$

This produces a regular and well-shaped initial parameterized F° under fixed boundary conditions. The parameters of the quadratic function, the length functional F_L and the uniformity functional F_U, are controlled by non-negative weights λ_L and λ_U. Their calculation formula is:

$$F_L(d^{\circ\ \tau}_{ij}) = \sum_{\tau=1}^{P} \int_{[0,1]^2} \left(\left\|D_uF^{(\tau)}\right\| + \left\|D_vF^{(\tau)}\right\|\right) dudv \tag{21}$$

$$F_U(d^{\circ\ \tau}_{ij}) = \sum_{\tau=1}^{P} \int_{[0,1]^2} \left(\left\|D_{uu}F^{(\tau)}\right\|^2 + 2\left\|D_{uv}F^{(\tau)}\right\|^2 + \left\|D_{vv}F^{(\tau)}\right\|^2\right) dudv \tag{22}$$

Based on the initial parameterization F° ,the desired compound surface parameterization F is generated by minimizing the following objective function:

$$F_2(d_{ij}^{(\tau)}) + \lambda_L F_L(d_{ij}^{(\tau)}) + \lambda_U F_U(d_{ij}^{(\tau)}) \to min \tag{23}$$

Where F_2 makes the constructed compound surface parameterization F close to the initial compound surface parameterization F° , calculated as follows:

$$F_2(d_{ij}^{(\tau)}) = \sum_{\tau=1}^{P} \int_{[0,1]^2} \left\|F^{(\tau)} - F^{\circ\,(\tau)}\right\|^2 dudv \tag{24}$$

Non-negative weights λ_L、$\lambda_U \in [1, \frac{1}{1000}]$ control the functional parameters length functional F_L and uniformity functional F_U [27] are used to obtain a good quality parameterization. The compound parameter domain surface before and after optimization is shown in Fig. 12. The compound parametric domain achieves G^1 continuity at the common boundary.

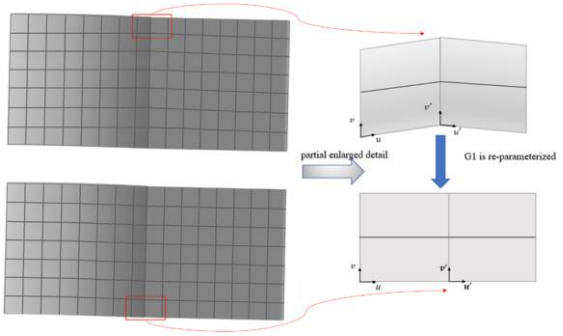

Figure 12. Local schematic of the compound parameter domain surface patch before and after G^1 optimization.

5. Results and discussion

The open blisk is a complex and representative component; Its blades feature high-curvature and smooth areas, with fillet transition zones at the blade fillets, fully reflecting the features of complex compound surfaces and continuity. This study first ensures the continuous machining of the compound surfaces (blades and fillets) on the open blisk. It verifies the continuity optimization of the tool paths at the common boundaries of the compound surfaces. The machining of the open blisk is typically designed for the fillet and the blades, and the two parts are shown in Fig. 13, respectively. In this study, Visual Studio 2022 is used as the development platform to propose a method to expand the open blisk blades and fillets horizontally into a compound surface consisting of eight trimmed surfaces (α_1⋯α_4， β_1⋯β_4) and vertically stitch them together, so that the blade and fillet of the open blisk form a compound surface ∅.

The compound surface consisting of trimmed surfaces (blades and fillets) is first reparameterized using the method described in Section 2, tool paths with C^0 continuity are then generated using the method proposed in Section 3 (the surface is C^1-continuous). Finally smooth tool paths are achieved through the continuity optimization method detailed in Section 4. The mapping of the compound surface ∅ on the Coons parameter domain is illustrated in Fig. 14, where it can be seen that each of the trimmed surfaces takes values in the range [0,1].

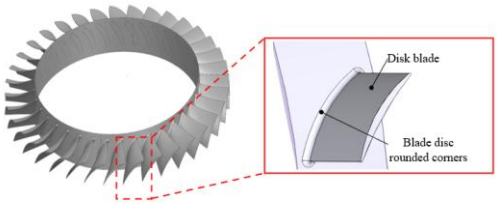

Figure 13. Schematic diagram of the open blisk and the open blisk blade and rounded corners on the blade.

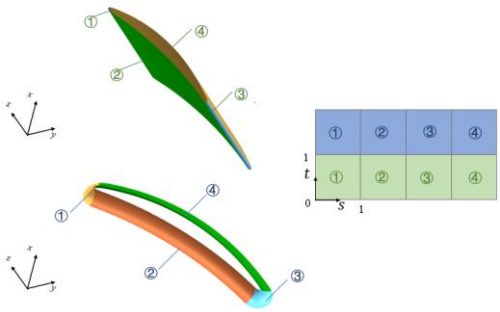

Figure 14. Schematic mapping of the complex surface ∅ on the Coons parameter field.

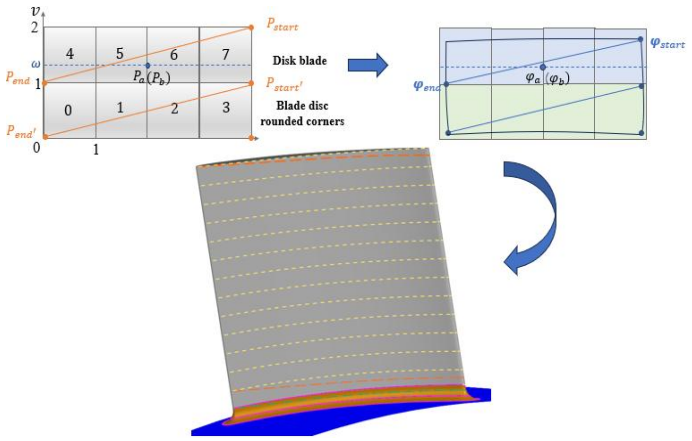

Figure 15. Spiral machining tool path generation for compound curved surfaces in Euclidean space.

Take a point P_a on the right boundary of the ith surface $F^{(i)}$, and take a point P_b at the same value on the left boundary of the $i+1$th surface $F^{(i+1)}$, then we can see that the two points are coincident, i.e., $P_a = P_b$. Mapping back to UV parameter domain, the two points are still coincident; at this time, there is $\varphi_a = \varphi_b$. Connecting P_{start} and P_{end} points in the Coons parameter domain with a straight line, the position of P_{start} and $P_{start'}$ are shown in Fig.14.The two points coincide because the compound surfaces are connected at the beginning and the end. Mapping the oblique lines on the Coons surface back into Euclidean space results in a series of spirally arranged cutter contact curves, as shown in Fig. 15.

In the two-dimensional UV parameter domain in Euclidean space, the paths at the surface splices may produce nonsmooth phenomena. The method described in Section 4 is used to construct a new G^1-continuous parameter surface within the open blisk blade compound UV parameter domain so that the paths on the open blisk blade compound surface in Euclidean space are C^1-continuous. In the experiment, the coordinates of each machining point along the tool path were determined by mapping points from the previously mentioned UV parameter domain. This method ensures consistency between the continuity of the parameter domain and the smoothness of the curve in Euclidean space. In this study, the above work is verified through simulation in Visual Studio 2022, and the results in Fig. 16 clearly demonstate smooth contrast of the paths. Fig. 16 (a) shows the simulation results of the tool path generated by reconstructing the G^1-continuous compound surface with the UV parameter domain, while Fig. 16 (b) shows the simulation results of the tool path generated from the initial

G^0 compound UV parameter domain.

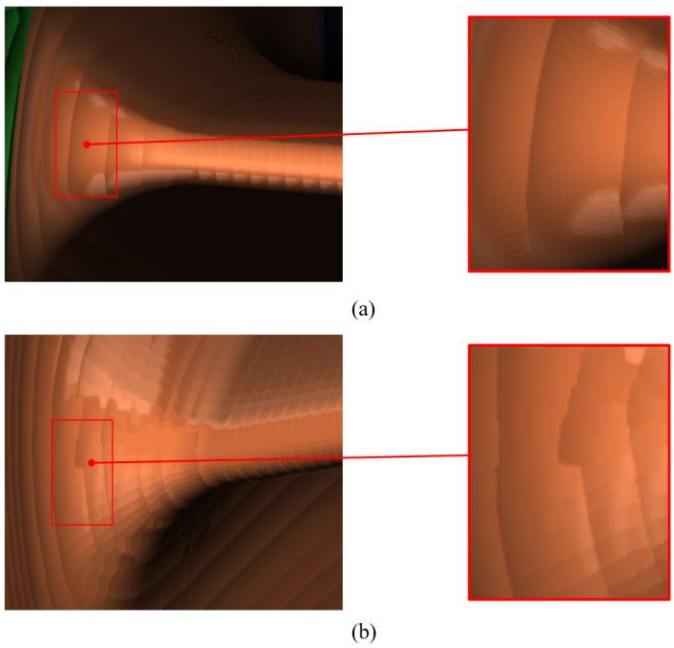

Figure 16. Tool path simulation of compound surface before and after optimization (a) Tool path simulation generated by parametric domain reconstruction of G^1-continuous compound surface (b) Tool path simulation generated by the initial G^0 compound parametric domain.

Before machining, the toolpaths for the reconstructed G^1 continuous compound surface and the initial G^0 continuous compound surface within the UV parameter domain were simulated in Visual Studio 2022. Simulation results indicate that both residual and overcutting in the machining toolpath within the reconstructed G^1 continuous compound parameter domain remain below $0.02mm$. Additionally, the reconstructed surface exhibits better smoothness and machining accuracy at the common boundary of the compound surfaces, far surpassing the machining simulation results of the toolpath generated on the initial G^0 compound surface, as shown in Fig. 17.

The above work is experimentally verified on the Mikron machine tool UCP800 to finish the open blisk. The three-dimensional morphology at the fillets of the machined blade is measured under the white light interferometer. The actual machining diagrams before and after the optimization, three-dimensional morphology diagrams, and roughness data diagrams are shown in Fig.18, respectively, as $Ra_{before} = 0.850$ and $Ra_{after} = 0.627$; the average roughness depth before and after the optimization is $Rz_{before} = 4.823$, $Rz_{after} = 4.232$. According to the above data, it can be concluded that the roughness after the optimization is reduced by 18%, and the roughness depth is decreased by 12.3% after optimization compared to before. The experiment demonstrates that the proposed method achieves higher accuracy and superior surface machining quality when machining the blade compound surface.

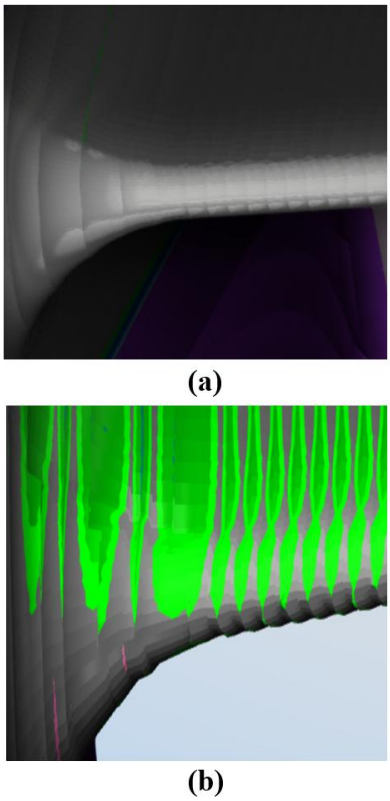

Overcut

Range(mm)	Color
0.800	Red
0.700	Brown
0.600	Yellow
0.500	Orange
0.200	Maroon
0.050	Magenta
0.020	Pink
0.000	Gray

Residual

Range(mm)	Color
0.800	Steel Blue
0.700	Olive Green
0.600	Purple
0.500	Light Blue
0.200	Green
0.050	Dark Blue
0.020	Neon Green
0.000	Gray

Figure 17. Simulation results of toolpath planning in Vericut for the reconstructed G^1 continuous parameter domain and the initial compound G^0 parameter domain.

The contour accuracy of the blade surface was measured using a CMM, and the accuracy graphs before and after optimization are shown in Fig. 19. The contour accuracy judgment data values were calculated. From Table 1, it can be concluded that the average value after optimization is 11.6% lower than that before optimization. Additionally, the closer the average value is to the target value (usually 0), the higher the machining accuracy is; the standard deviation after optimization is 4.9% lower than that before optimization, which indicates that the machining process is more stable after optimization.

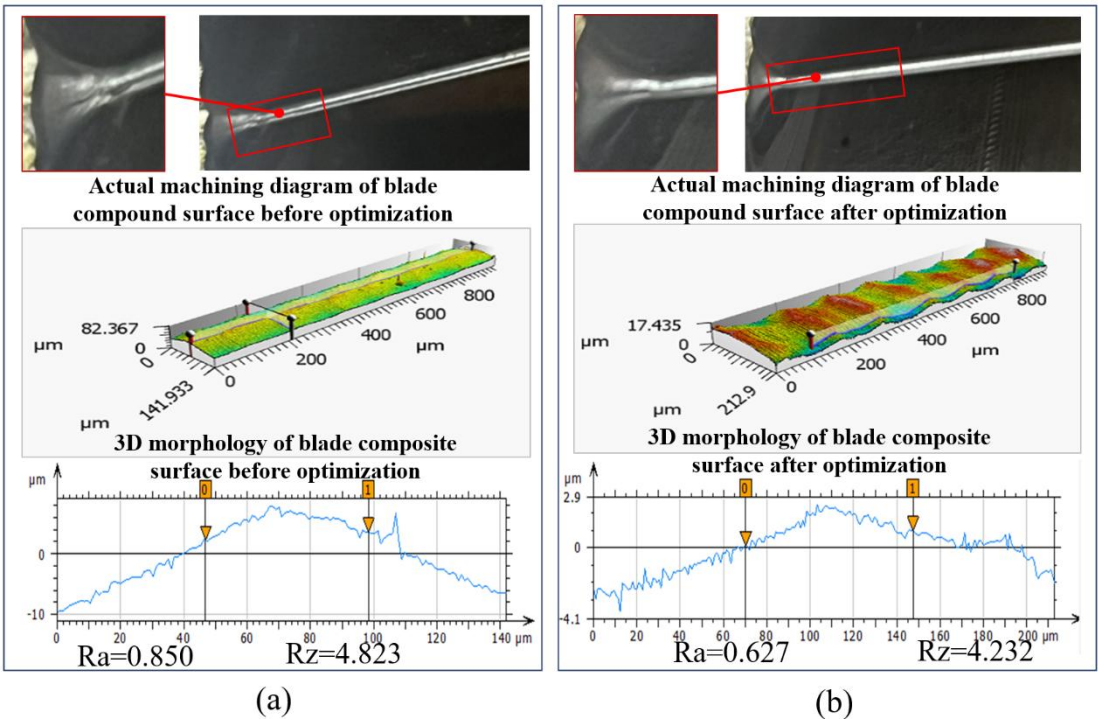

Figure 18. Data plots of actual machining, 3D topography, and roughness(a) before optimization (b)after optimization.

Table 1. Comparative analysis of blade compound surface contour accuracy before and after optimization.

	Mean value (mm)	Standard deviation	Minimum value (mm)	Maximum value (mm)
Before optimization	0.02592	0.00926	0.01132	0.04922
After optimization	0.02292	0.00881	0.01152	0.04712

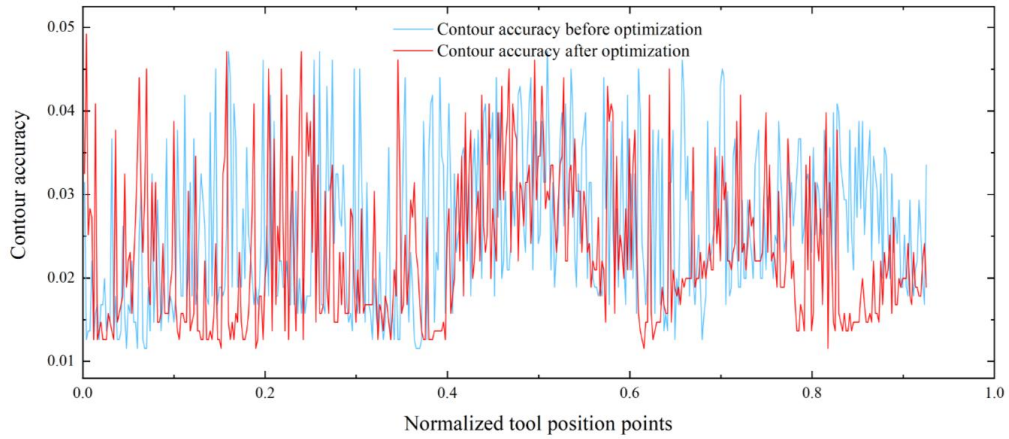

Figure 19. Compound surface contour accuracy before and after optimization.

5. Conclusions

In this paper, a way to fit the 2D parameter domain of 3D surfaces in Euclidean space based on 2D Coons surfaces is proposed for the generation of spiral machining tool paths on compound and trimmed surfaces, and the spiral paths of the compound surfaces are generated directly with the help of Coons surfaces by a two-step mapping, which reduces the steps of the path generation. However, at this time, the generated path at the common boundary of the compound surface does not necessarily ensure C^1 continuity, in the case of specifying the compound surface in the Euclidean space as C^1 continuity, the idea in [16] is adopted to reconstruct the compound parameter domain with G^1 continuity by using the Coons mapping in the initial 2D parameter domain to ensure that the tool path at the common boundary of the compound patch in the 2D parameter domain is G^1 continuity, which then enables the C^1 continuity

of the path at the common boundary of the compound surface in Euclidean space. The research method is applied in machining open blisk blades and fillets compound surfaces of the open blisk. The experimental results show that the surface roughness of the machined parts after optimization is reduced by 18% compared with that before optimization, and the depth of surface roughness is reduced by 12.3%. The machining accuracy and surface quality of the parts are improved.

Acknowledgement

This work is supported by National Key Research and Development Program of China (No. 2022YFA1005204).

References

1. Liang Q, Wang Y, Fu H, Han Z. Cutting path planning for ruled surface impellers. Chinese Journal of Aeronautics 2008; 21(5): 462–471. https://doi:10.1016/S1000-9361(08)60060-6.
2. Zhang K, Tang K. An efficient greedy strategy for five-axis tool path generation on dense triangular mesh. The International Journal of Advanced Manufacturing Technology 2014; 74: 1539–1550. https://doi: 10.1007/s00170-014-6083-1.
3. Feng H, Teng Z. Iso-planar piecewise linear NC tool path generation from discrete measured data points. Computer-Aided Design 2005; 37(1): 55–64. https://doi: 10.1016/j.cad.2004.04.001.
4. He W, Lei M, Bin H. Iso-parametric CNC tool path optimization based on adaptive grid generation. The International Journal of Advanced Manufacturing Technology 2009; 41: 538–548. https://doi.org/10.1007/s00170-008-1500-y
5. Feng H, Li H. Constant scallop-height tool path generation for three-axis sculptured surface machining. Computer-Aided Design 2002; 34(9): 647–654. https://doi:10.1016/S0010-4485(01)00136-1.
6. Lee E. Contour offset approach to spiral toolpath generation with constant scallop height. Computer-Aided Design 2003; 35(6): 511-518. https://doi: 10.1016/S0010-4485(01)00185-3.
7. Sun Y, Guo D, Jia Z, Wang H. Iso-parametric tool path generation from triangular meshes for free-form surface machining. The International Journal of Advanced Manufacturing Technology 2006; 28(7): 721–726. https://doi.org/10.1007/s00170-004-2437-4.
8. Xu J, Ji Y, Sun Y, Lee Y. Spiral tool path generation method on mesh surfaces guided by radial curves. Journal of Manufacturing Science and Engineering 2018; 140(7): 071016. https://doi.org/10.1115/1.4039918.
9. Guo J, Ding F, Jia X, Yan D. Automatic and high-quality surface mesh generation for CAD models. Computer-Aided Design 2019; 109: 49–59. https://doi.org/10.1016/j.cad.2018.12.005.
10. Suresh K, Yang D C H. Constant scallop-height machining of free-form surfaces. Journal of engineering for industry 1994; 116(2): 253–259. https://doi: 10.1115/1.2901938.
11. Yang, D C H, Chuang J, OuLee T H. Boundary-conformed toolpath generation for trimmed free-form surfaces. Computer-Aided Design 2003; 35(2): 127–139. https://doi: 10.1016/S0010-4485(02)00047-7.
12. Chuang J, Yang D C H. A laplace-based spiral contouring method for general pocket machining. In ASME International Mechanical Engineering Congress and Exposition 2004; 47136: 227–236. https://doi: 10.1115/IMECE2004-60138.
13. Takasugi K, Asakawa N. Parameter-based spiral tool path generation for free-form surface machining. Precision Engineering 2018; 52: 370–379. https://doi: 10.1016/j. precisioneng.2018.01.013.
14. Xu J, Sun Y, Wang S. Tool path generation by offsetting curves on polyhedral surfaces based on mesh flattening. The International Journal of Advanced Manufacturing Technology 2013; 64: 1201–1212. https://doi: 10.1007/s00170-012-4075-6.
15. Han J, Du H, Tian X, Xia L. Research on spiral finishing path generation for integral blade disc composite surface blades based on coons reparameterization. Chinese Journal of Mechanical Engineering 2025; 1–19. https://link.cnki.net/urlid/42.1294.th.20250514.1959.006.
16. Randrianarivony M. On global continuity of Coons mappings in patching CAD surfaces. Computer-Aided Design 2009; 41(11): 782–791. https://doi: 10.1016/j.cad.2009.04.012.
17. Kapl M, Vitrih V, Jüttler B, Birner K. Isogeometric analysis with geometrically continuous functions on two-patch geometries. Computers & Mathematics with Applications 2015; 70(7): 1518–1538. https://doi: 10.1016/j.camwa.2015.04.004.
18. Collin A, Sangalli G, Takacs T. Analysis-suitable G^1 multi-patch parametrizations for C^1 isogeometric spaces. Computer Aided Geometric Design 2016; 47: 93–113. https://doi: 10.1016/j.cagd.2016.05.009.
19. Kapl M, Sangalli G, Takacs T. Construction of analysis-suitable G1 planar multi-patch parameterizations. Computer-Aided Design 2018;

97: 41–55. https://doi: 10.1016/j.cad.2017.12.002.

20. Elber G, Cohen E. Tool path generation for freeform surface models. In Proceedings on the second ACM symposium on Solid modeling and applications 1993; 419–428. https://doi: 10.1145/164360.164500.
21. Feng H, Li H. Constant scallop-height tool path generation for three-axis sculptured surface machining. Computer-Aided Design 2002; 34(9): 647–654. https://doi: 10.1016/S0010-4485(01)00136-1.
22. Yazıcı İ, Yaylacı E K, Yalçın F. Modified golden section search based MPPT algorithm for the WECS. Engineering Science and Technology, an International Journal 2021; 24(5): 1123–1133. https://doi: 10.1016/j.jestch.2021.02.006.
23. Zhang Y, Ji Y, Zhu C. Multi-patch parameterization method for isogeometric analysis using singular structure of cross-field. Computers & Mathematics with Applications 2024; 162: 61–78. https://doi.org/10.1016/j.camwa.2024.03.001.
24. Sun Y, Sun S, Xu J, Guo D. A unified method of generating tool path based on multiple vector fields for CNC machining of compound NURBS surfaces. Computer-Aided Design 2017; 91: 14–26. https://doi: 10.1016/j.cad.2017.04.003.
25. Wang L, Zhu X, Tang Z. Coons type blended B-spline (CNSBS) surface and its conversion to NURBS surface. Computers & Graphics 1997; 21(3): 297–303. https://doi: 10.1016/S0097-8493(97)00006-X.
26. Peters J. Geometric Continuity. In: Handbook of computer aided geometric design. Amsterdam: North-Holland 2002; 193–227.
27. Buchegger F, Jüttler B. Planar multi-patch domain parameterization via patch adjacency graphs. Computer-Aided Design 2017; 82: 2–12. https://doi: 10.1016/j.cad.2016.05.019.